# Oscillator Priming and Preoscillation Noise in a Gyrotron

ALAN H. McCURDY AND CARTER M. ARMSTRONG

*Abstract*—**Phase control is achieved in a pulsed gyrotron oscillator both by applying an external priming signal directly to the oscillator and by applying the signal to a prebunching cavity. A pulse-to-pulse phase jitter of $< 2.5°$ is achieved in the gyrotron at drive-to-oscillator power ratios of $-36.6$ dB (drive signal-to-noise power ratio of 36 dB) in the direct injection case and $-71$ dB (drive signal-to-noise power ratio of 22 dB) in the prebunched case. A lumped element theory is compared to the experimental results. The theoretical description seems valid when the drive frequency is within about 5 MHz of that of the oscillator. Preoscillation noise in the gyrotron is $\sim 1.0$ μW, larger than expected from either shot noise or thermal noise but in the vicinity of spontaneous cyclotron emission. Convective RF noise growth is investigated. No evidence of the electrostatic cyclotron instability is seen. All growth observed can be attributed to the gyroklystron amplification mechanism. However the noise growth per unit length is not as large as that of a narrow-band drive signal. Thus a prebuncing system is advantageous for achieving control over the oscillation buildup in a pulsed gyrotron.**

## I. Introduction

THERE IS a need for coherent RF sources in the millimeter and submillimeter wavelength range. Though gyrotron oscillators (based on the cyclotron resonance maser mechanism) have demonstrated high power [1], [2] and high efficiency [3], many applications, including RF particle acceleration and phase coherent radar, require phase control, which the free oscillator cannot provide. Oscillator priming [4], [5] is one method used to achieve phase control in pulsed microwave devices. This method involves injection of a small external signal into the oscillator during the oscillation buildup. The result is that each output pulse of the oscillator starts up in phase with the external signal.

Priming is to be distinguished from injection phase locking in that the priming effect may occur at much lower external signal levels and yields no frequency control over the oscillator [6], [7]. It is possible that phase control of a powerful (e.g. $\sim 1$ GW) millimeter wavelength oscillator may be more easily accomplished via priming than by phase locking. Since phase locking requires a relatively large external signal (usually no smaller than 20 dB below the oscillator power), a chain of phase-locked external sources is needed. A simpler solution is to use a single driver to prime the oscillator (typical priming powers for 2° pulse-to-pulse phase control are 20 to 30 dB below that for phase locking). Coupling the priming system to a phase-locked loop [8] to provide intrapulse frequency control may yield the same degree of oscillator control as the phase-locked system.

Manuscript received July 3, 1987; revised November 30, 1987. This work was supported by the U.S. Office of Naval Research and the Office of Naval Technology.

The authors are with the Electronics Science and Technology Division, Naval Research Laboratory, Washington, DC 20375.

IEEE Log Number 8819962.

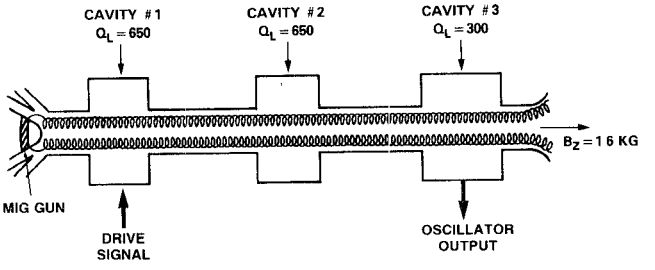


Fig. 1. Three-cavity gyroklystron configuration.

The generation of noise in the electron beam formed by MIG guns in gyro-oscillators and amplifiers has not been thoroughly investigated. Mechanisms of noise generation and growth are important because noise compromises the phase stability of amplifiers and the frequency stability of oscillators. Once the mechanisms are recognized, the gun and circuit designs can consider methods of noise suppression. In this work, preoscillation noise values are determined from jitter measurements of oscillation startup time in the gyrotron. These noise calculations are also required for characterization of the priming phenomenon.

Two methods of priming the gyrotron are investigated: (1) directly injecting the external signal into the cavity oscillator and (2) injecting the signal into a premodulation cavity and then allowing the bunched electron beam to prime the oscillator. The system used is a three-cavity gyroklystron configuration [9], shown in Fig. 1. In this system any of the cavities can be made to oscillate by appropriate adjustment of the axial magnetostatic field and cavity resonance.

The priming effect can be seen in Fig. 2. The three signals shown in each oscilloscope photograph are (from top), the gyrotron RF output signal, the external drive signal, and a mixer signal that displays the relative phase angle between the drive and gyrotron. If the drive signal is not applied during the correct instant in the oscillation *buildup*, then there is no pulse-to-pulse phase control, as shown in (a) and (b) of Fig. 2. The widened drive pulse and incoherent mixer output in Fig. 2(b) show that there is no control of the steady-state oscillation by the drive signal. In Fig. 2(c), where the drive pulse is slightly earlier in time than in Fig. 2(b), the gyrotron is primed and each

0018-9480/88/0500-0891$01.00 

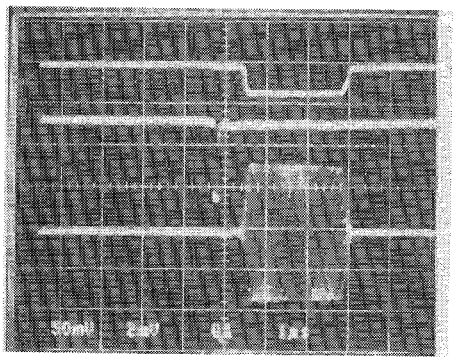

(a)

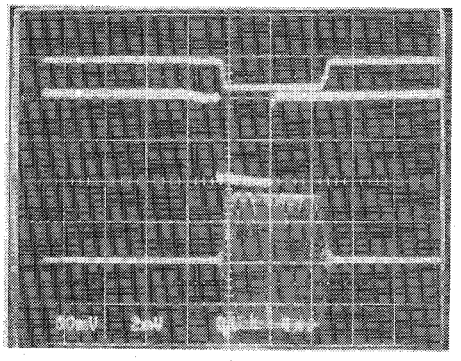

(b)

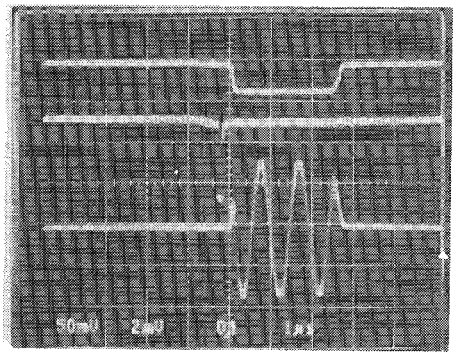

(c)

Fig. 2. Experimental observation of the priming phenomenon. The three traces are, from top to bottom, gyrotron RF output, pulsed external drive signal, and phase diagnostic output. In (a) the drive pulse arrives too early. In (b) the drive pulse is widened but too late. In (c) the drive pulse arrives during the oscillation buildup and primes the oscillation, as can be seen from the steady output of the phase diagnostic.

oscillation pulse starts up in phase synchronism with the drive signal. The continual, intrapulse phase slippage is due to a frequency difference between the drive signal and the gyrotron.

## II. Priming Theory

The theory of oscillator priming presented here is closely related to the simple theory developed for magnetrons [4] and more recently applied to lasers [10]. A lumped element approximation is used so that the output of the gyrotron can be represented by a complex voltage developed at a suitable reference plane in the output waveguide. Fig. 3 shows the equivalent circuit for the gyrotron oscillator as seen from the position of the detuned short. This representation is justified for analysis of the behavior of the one-port gyrotron cavity near its resonant frequency (assuming that propagation effects are not dominant). In addition, there is substantial spacing between cavity modes so that the circuit parameters can be unambiguously defined. The quantities $G_{\text{wall}}$, $C$, and $L$ model the empty gyrotron cavity. The cold cavity resonant frequency is given in terms of the energy storage elements as $1/\sqrt{LC}$. The cavity wall losses are represented by the shunt conductance $G_{\text{wall}}$. $Y_b$ is the electron beam admittance, which is the current-to-voltage ratio excited at the reference plane by the electron beam–electromagnetic wave interaction. Finally $Y_L$ is the external load admittance seen from the reference plane. Since the gyrotron operates into a matched load, the load admittance is related to the shunt wall conductance by the coupling coefficient $\beta$ of the iris between the cavity and the output waveguide. The calculation is carried out by comparing voltages developed across the wall conductance. Thus all RF power input through the waveguide or measured across the output load must be corrected by the coupling coefficient before being introduced into the calculation.

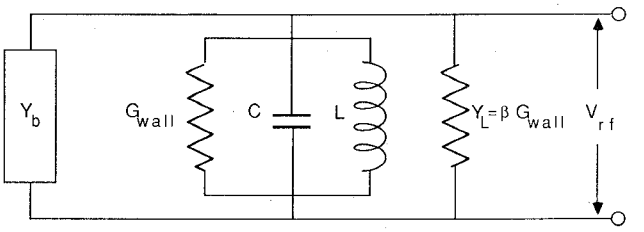


Fig. 3. Equivalent circuit of gyrotron oscillator. $Y_b$ and $Y_L$ are the beam and load admittances; $G_{\text{wall}}$, $C$, and $L$ are the cavity parameters and $V_{\text{RF}}$ is the voltage at the output reference plane.

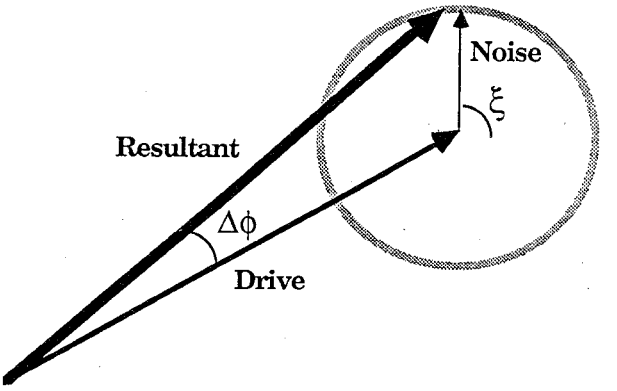


Fig. 4. Phasor diagram of voltage signals during initiation of oscillation. Noise varies randomly in phase and statistically in amplitude. Drive signal constrains possible initial oscillation phase to $\pm \Delta\phi$.

The effect of the external drive signal on the oscillation will be considered to be instantaneous. This assumption is justified because the external signal is very small compared to the oscillation at all times except during the very earliest part of the oscillation growth (steady-state oscillation amplitude $\gg$ drive signal amplitude). Thus the drive signal will be considered as merely modifying the initial condition from which the oscillation grows. Fig. 4 shows a

phasor diagram that predicts the oscillator initial condition. In the absence of the external signal, the oscillator starting voltage varies randomly in phase, as shown by the circle, and statistically in amplitude from pulse to pulse. The variation in amplitude $V$ is assumed to be described by the Rayleigh distribution:

$$P(V)\,dV = \frac{2V}{\overline{V^2}} \exp\left(-\frac{V^2}{\overline{V^2}}\right) dV \tag{1}$$

which has been shown to be applicable, with certain restrictions [11], to system containing a large number of oscillators. The many gyrating electrons in the oscillator cavity constitute the oscillator ensemble in the gyrotron system. The mean square noise amplitude is given by $\overline{V^2}$. In the case where the drive signal is present, the oscillator grows from the vector sum of the noise and drive signal. It can be seen from Fig. 4 that this vector varies over a more restricted range of phases (from $-\Delta\phi$ to $+\Delta\phi$) than in the undriven case. As the drive signal becomes larger in size relative to the noise, the pulse-to-pulse fluctuations in initial amplitude and phase decrease. Since the oscillation grows from the resultant amplitude, even within one e-folding time ( ~ 35 ns), the oscillator component is twice the drive. This strengthens our assumption that the drive signal is of comparable size to the oscillation for only a very brief period.

To calculate the effect of the drive signal on the oscillator, one must find the change in the probability distribution of starting phase angle as a function of drive power. The probability density of the oscillation starting at a particular phase $\phi$ in the driven case has been given by David [4]:

$$P\left(\phi,\overline{S^2}\right) = \frac{1}{2\pi}\left\{\left(|A+B|+|A-B|+\exp\left(-\frac{1}{\overline{S^2}}\right)\right.\right.$$
$$\left.\left. + \sqrt{\frac{\pi}{\overline{S^2}}}\cos\phi\exp\left(-\frac{\sin^2\phi}{\overline{S^2}}\right)\left(1-\operatorname{erf}\left(\frac{1}{\sqrt{\overline{S^2}}}\right)\right)\right)\right\}$$
$$\text{for } 0 \leqslant \phi \leqslant \pi/2$$

where

$$A = \exp\left(-\frac{\sin^2\phi}{\overline{S^2}}\right) - \exp\left(-\frac{1}{\overline{S^2}}\right)$$

and

$$B = \sqrt{\frac{\pi}{\overline{S^2}}}\cos\phi\exp\left(-\frac{\sin^2\phi}{\overline{S^2}}\right)\operatorname{erf}\left(\frac{\cos\phi}{\sqrt{\overline{S^2}}}\right)$$

$$P\left(\phi,\overline{S^2}\right) = \frac{1}{2\pi}\left(\exp\left(-\frac{1}{\overline{S^2}}\right) + \sqrt{\frac{\pi}{\overline{S^2}}}\cos\phi\exp\left(-\frac{\sin^2\phi}{\overline{S^2}}\right)\right.$$
$$\left.\cdot\left[1-\operatorname{erf}\left(\frac{1}{\sqrt{\overline{S^2}}}\right)\right]\right) \qquad \text{for } \pi/2 \leqslant \phi \leqslant \pi. \tag{2}$$

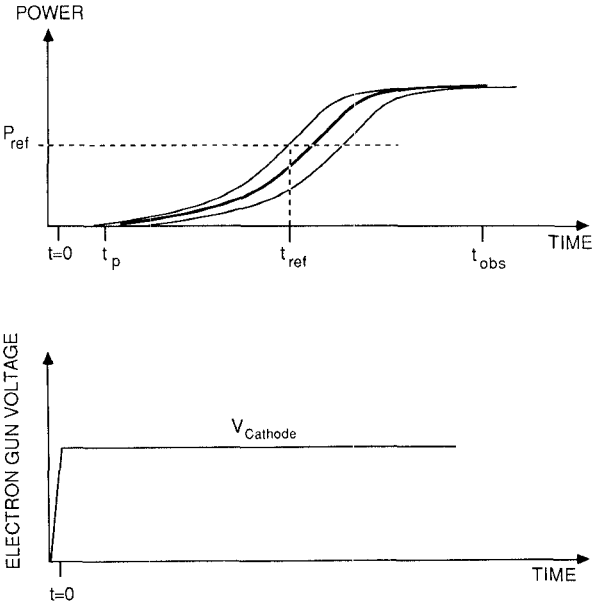


Fig. 5. Starting time jitter in gyrotron RF output. $t = 0$ is the time at which the MIG gun turns on. The CRM instability initiates at $t_p$ (also time of priming). $P_{ref}$ is an arbitrary power level. $t_{obs}$ is the time at which the phase jitter measurement is made.

Here $P$ is a function of the parameter $\overline{S^2}$, the mean square noise-to-signal power ratio, and (1) has been used in terms of power instead of amplitude (power being proportional to the square of the amplitude). The degree of phase control is related to the width of the distribution in (2). The variance is a measure of this width and is calculated by taking the square root of the dispersion:

$$\sigma_n^2 = \int_{-\pi}^{\pi} \left[\phi^2 - \phi_{\text{mean}}^2\right] P\left(\phi,\overline{S^2}\right) d\phi$$

and using the fact that $\phi_{\text{mean}} = 0$, since the distribution $P(\phi,\overline{S^2})$ is symmetric about $\phi = 0$. The variance can be determined as soon as the mean noise power is known.

The noise power is not calculated here from first principles, but is approximately determined from experimental measurements of the variation in startup time of the oscillation from pulse to pulse [12]. The noise is to be found at the time that the electron beam current and voltage reach the threshold of the cyclotron resonance maser instability. Through the small-signal regime, we assume that the oscillation amplitude grows exponentially:

$$P_{\text{ref}} = P\exp\left(\frac{t_{\text{ref}} - t_p}{\tau}\right). \tag{3}$$

Here $\tau$ is the growth rate, $P$ is the noise power (proportional to $V^2$) at $t = t_p$, $P_{\text{ref}}$ is an arbitrary small-signal reference power level, and $t_{\text{ref}}$ is the time (as measured from the leading edge of the flat-top portion of the high voltage pulse to the electron gun) that the oscillation reaches the reference power level (see Fig. 5). The time at which the oscillation begins to grow (and is primed) is $t_p$. The oscillation startup time is defined to be $t_{\text{ref}}$. Applying the temporal evolution of the noise voltage given by (3), the fluctuations in initial amplitude, described by (1),

translate into fluctuations in oscillation starting time $t_{\text{ref}}$ [13]:

$$f(t_{\text{ref}})\,dt_{\text{ref}} = \frac{P_{\text{ref}}}{\tau P_n}\exp\left(\frac{-(t_{\text{ref}}-t_p)}{\tau}\right) \cdot\exp\left[-\frac{P_{\text{ref}}}{P_n}\exp\left(\frac{-(t_{\text{ref}}-t_p)}{\tau}\right)\right]dt_{\text{ref}} \quad (4)$$

where $P_n$ is the mean noise power. $f(t_{\text{ref}})$ is the probability density of reaching $P_{\text{ref}}$ between $t_{\text{ref}}$ and $t_{\text{ref}}+dt_{\text{ref}}$. It can easily be shown that the width of this distribution is independent of the mean noise power level and is a function only of the oscillation growth rate. Therefore (unlike the calculation in [12]) we consider the variation in starting times in the *driven case* to determine the mean noise power. This new approach has the advantage of determining the noise power by comparing experiment with two features of the theoretical distribution, the mean and the width. In addition, relative measurements can be made by changing the drive power. This allows for more points of comparison.

When a driving signal is present during the early stages of oscillation buildup, the distribution function describing the initial oscillation amplitude is

$$P_d(V)\,dV = \frac{2V}{\overline{V^2}}\exp\left(-\frac{V^2+D^2}{\overline{V^2}}\right)I_0\left(\frac{2VD}{\overline{V^2}}\right)dV \quad (5)$$

where $D$ is the drive amplitude and $I_0$ is a modified Bessel function. Equation (5) is the sum of the constant drive vector (see Fig. 4) with the Rayleigh distributed noise [14]. $V$ is now the magnitude of the sum of the noise and drive voltages at $t=t_p$. The translation of this amplitude variation into starting time variation follows with the use of (3) ($P$ being still proportional to $V^2$):

$$f_d(t_{\text{ref}})\,dt_{\text{ref}} = \frac{R}{\tau\overline{S^2}}\exp\left(-\frac{t_{\text{ref}}-t_p}{\tau}\right) \cdot\exp\left(-\frac{R\exp\left(-\frac{t_{\text{ref}}-t_p}{\tau}\right)+1}{\overline{S^2}}\right) \cdot I_0\left[\frac{2\sqrt{R}}{\overline{S^2}}\exp\left(-\frac{t_{\text{ref}}-t_p}{2\tau}\right)\right]dt_{\text{ref}}$$

where

$$R = \frac{P_{\text{ref}}}{P_d}. \quad (6)$$

The new distribution function $f_d(t_{\text{ref}})$, analogous to (4) for the undriven case, has a width and a mean that depend on drive power. In principle, the noise power should be inferred by using the complete distribution function $f_d(t_{\text{ref}})$. However, we experimentally measure only two characteristics of the distribution, the mean and the width.

## III. Experimental

### A. System Description

The gyroklystron configuration, Fig. 1, consists of three rectangular $TE_{101}$ mode cavities separated by drift sections that are cut off to the 4.5 GHz oscillation frequency. The first two cavities are identical in construction and are about 20 percent shorter than the last cavity. The electron gun supplies a current of 6 A at a voltage of 30 kV in 4.0 $\mu$s pulses at a 60 Hz repetition rate. The perpendicular-to-parallel velocity ratio $\alpha$ of the electron beam is between 1.0 and 1.5, depending on the magnetic field near the electron gun. Simulations of the electron gun predict the electron guiding centers to be approximately uniformly distributed on a circle $\sim 0.94$ cm in radius. The output RF power is near 2 kW when either of the first two cavities is used as the gyrotron oscillator and near 20 kW when the third cavity is used. Direct injection experiments are performed using an oscillation in the second cavity with an external signal launched through its output waveguide. A sweep oscillator with a 20 W TWT amplifier comprise the external signal source. Special care is taken to ensure that no oscillator output feeds back into the external source. Circulators are used to provide $>80$ dB isolation. Since very small drive powers are required to prime an oscillator, even very small feedback signals from the oscillator are comparable in size to the drive signal and may effect source performance. The problem is avoided in this experiment by operating the driver at a high output power ($\sim 5$ W) and attenuating the drive signal by 50 or 60 dB before injection into the gyrotron. This method has the added benefit of providing more isolation between the driver and the oscillator.

The premodulation experiments are carried out by injecting the external signal into the first cavity of the gyroklystron configuration and priming an oscillation in the third cavity. The isolation between oscillator and driver is not as severe in this case since each of the drift sections provide $\sim 30$ dB isolation at 4.5 GHz.

### B. Noise Power Measurement

The gyrotron noise power is inferred from a measurement of pulse-to-pulse jitter in gyrotron oscillator starting time (time at which the oscillation reaches $P_{\text{ref}}$). This measurement is made by enveloping the voltage signal of a crystal diode that monitors the gyrotron output power. Typical results of this measurement are shown in Fig. 6 for an experiment using one prebunching cavity. The reduction in thickness of the oscillation front edge is a clear indication of a reduction in starting time jitter due to the injected signal. Since 100 waveforms are saved on the oscilloscope, the width of the front edge is approximately that between the 0.5 percent and 99.5 percent points of the distribution function $f_d(t)$. It is assumed here that only 1/100, or 1 percent, of the distribution remains unsampled.

The mean starting time is measured by averaging the crystal diode output over 100 waveforms. The averages for

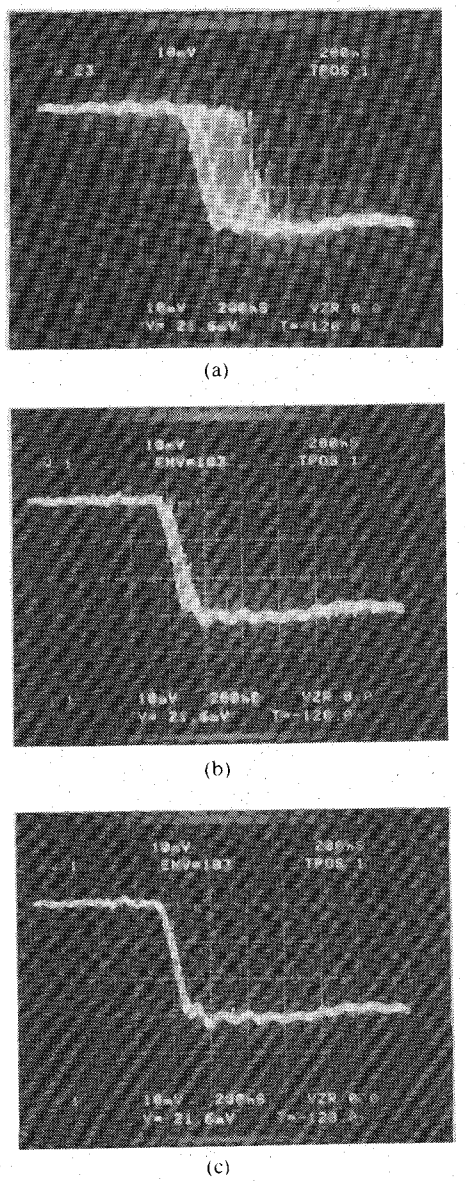

(a) (b) (c)

Fig. 6. Reduction of starting time jitter by priming. (a) free oscillation. (b) $P_{drive}/P_{osc} = -72.7$ dB. (c) $P_{drive}/P_{osc} = -65.8$ dB. Beam voltage = 27.1 kV; beam current = 4.9 A; output power = 800 W; drive frequency = oscillation frequency.

three different drive power levels are also shown in the oscillographs of Fig. 6 as the bright lines inside the envelopes. As the drive power is increased, the average position of the oscillation front edge moves to the left (to earlier times). This corresponds to a decrease in the mean starting time with an increase in drive power.

### C. Interpretation of the Phase Diagnostic

The priming phenomenon, as has been described, is one of degree as opposed to the discontinuous phenomenon of phase locking. There is no threshold for the onset of priming. Our measure of "goodness" of priming is the variance of $P(\phi, \overline{S^2})$. The smaller this variance, the less pulse-to-pulse phase jitter expected. The relative phase is measured by mixing the drive signal and the gyrotron output in phase quadrature [15]. The mixer IF signal is displayed directly on a digital oscilloscope. The variation in relative phase is measured about 200 ns after the gyrotron oscillation reaches steady state. A system controller automatically records the relative phase of each pulse and does the statistical analysis.

Several effects must be taken into account to deduce the phase jitter from the raw data provided by the mixer phase diagnostic. Compensation must be made for the line lengths to the LO and RF mixer ports and for the time delay between the start of the pulse and the time of the measurement. Since these effects do not vary from pulse to pulse, they can be compensated for by an appropriately adjusted phase shifter in one of the lines to the mixer input ports. However the pulse-to-pulse starting time jitter and pulse-to-pulse variations in gyrotron oscillator frequency produce a phase jitter which is not correctable. Finally, the output of the phase diagnostic is actually the sine of the relative phase angle between the drive signal and gyrotron instead of the angle itself.

The interpretation of the diagnostic output follows. The relative phase between the gyrotron oscillator and the drive signal at the mixer is

$$\phi_{rel} = \phi_n + (\omega - \omega_d)(t_{obs} - t_p) + \phi_{P.S.} + \phi_{P.L.} \qquad (7)$$

where $\phi_n$ is the phase jitter due to the noise from which the oscillation grows, $\phi_{P.S.}$ is the phase shifter contribution, and $\phi_{P.L.}$ is the shift due to path length effects. The time of measurement is $t_{obs}$, $t_p$ is the time that the gyrotron oscillation starts to grow (the time that the initial condition is imposed), and $\omega$ and $\omega_d$ are the gyrotron oscillator and drive signal frequencies. Time is measured, as before, from the leading edge of the high voltage pulse (see Fig. 5). Pulse-to-pulse variations in the high voltage startup were orders of magnitude below that of the oscillation. The frequency-dependent term in (7) represents the phase shift due to a change in oscillation frequency. We arrive at this term after a calculation of the total elapsed phase in the gyrotron oscillator and drive signal from $t = 0$. The oscillator phase changes by

$$\phi_0(t_{obs}) = \omega_d t_p + \omega(t_{obs} - t_p) + \phi_n \qquad (8)$$

between $t = t_{obs}$ and $t = 0$. Here we assume that the gyrotron oscillator output changes frequency from $\omega_d$ to $\omega$ at the time of priming. This instantaneous frequency change is consistent with our assumption that the oscillation experiences rapid growth and soon dominates the drive signal. The phase of the oscillator at the instant of priming is $\phi_n$. The phase of the drive signal at $t = t_{obs}$ is

$$\phi_d(t_{obs}) = \omega_d t_{obs} \qquad (9)$$

where the initial phase of the drive signal has been taken to be zero. The difference between (8) and (9) gives the relative phase between the gyrotron oscillation and drive signal at $t = t_{obs}$ and is just the first two terms of (7).

The phase shifter is adjusted to compensate for all phase shifts which do not vary from pulse to pulse. This leaves a small phase angle which varies about zero. Thus

$$\phi_{P.S.} = -(\omega_{mean} - \omega_d)(t_{obs} - t_p) - \phi_{P.L.} \qquad (10)$$

and the remaining jitter phase is

$$\phi_{\text{rel}} = \phi_n + (t_{\text{obs}} - t_p)(\omega - \omega_{\text{mean}}). \tag{11}$$

Here $\omega_{\text{mean}}$ is the mean free oscillation frequency. The phase shifter is adjusted as either the drive frequency or the drive power is changed. The drive power level enters (10) through $t_{\text{obs}}$. Since the measurement is always made ~ 200 ns into the saturated part of the RF pulse, $t_{\text{obs}}$ must be changed as drive power changes cause the oscillation startup time to vary. The time at which the oscillator is primed can be seen from Fig. 2 to be about 300 ns before the oscillation saturates. The uncertainty in this measurement is perhaps as large as 50 ns but the priming results are not very sensitive to $t_p$.

The actual mixer output is the sine of the relative phase angle. Hence the dispersion of the output of the mixer is

$$\overline{\chi^2} = \int\int \left[\chi^2 - \chi^2_{\text{mean}}\right] P\left(\phi_n, \overline{S^2}\right) G(\omega)\, d\phi_n\, d\omega$$

where

$$\chi = \sin\phi_{\text{rel}}. \tag{12}$$

Using (11), the dispersion of $\chi$ becomes

$$\overline{\chi^2} = \langle \sin^2\phi_n \rangle_\phi \left\langle \cos^2\left[\Delta t(\omega_{\text{mean}} - \omega)\right]\right\rangle_\omega + \langle \cos^2\phi_n \rangle_\phi \left\langle \sin^2\left[\Delta t(\omega_{\text{mean}} - \omega)\right]\right\rangle_\omega. \tag{13}$$

Here the abbreviations

$$\langle J \rangle_\phi = \int_{-\pi}^{\pi} P\left(\phi_n, \overline{S^2}\right) J\, d\phi_n$$

$$\langle J \rangle_\omega = \int_{-\infty}^{\infty} G(\omega) J\, d\omega$$

$$\Delta\omega = \omega_{\text{mean}} - \omega_d \quad \text{and} \quad \Delta t = t_{\text{obs}} - t_p$$

have been used. The distribution in oscillation frequency is assumed to be Gaussian:

$$G(\omega) = \frac{1}{\sqrt{2\pi}\,\omega_{\text{rms}}} \exp\left[-\frac{1}{2}\left(\frac{\omega - \omega_{\text{mean}}}{\omega_{\text{rms}}}\right)^2\right]. \tag{14}$$

In the limit where the fluctuations in phase $\phi_n$ and frequency $(\omega_{\text{mean}} - \omega)$ are very small, (13) becomes

$$\overline{\chi^2} = \langle \phi_n^2 \rangle_\phi + \left\langle \Delta t^2 (\omega_{\text{mean}} - \omega)^2 \right\rangle_\omega$$

where the sine and cosine terms have been expanded to first order in the small terms. In this limit the variables $\phi_n$ and $\Delta t(\omega_{\text{mean}} - \omega)$ are uncorrelated. The error introduced due to the neglect of pulse-to-pulse variations in oscillation amplitude is found to be only a fraction of a percent. It can be shown that if the gyrotron oscillation and drive signals are completely unrelated in phase, then the variance of the diagnostic output will be 0.707.

## IV. Results and Discussion

### A. Noise Power in the Gyrotron

The noise power generated by the electron beam as oscillation is approached is evaluated in this experiment using oscillations in each of the three cavities and using two- and three-cavity systems. This investigation is made to determine several critical features of the beam noise. These include the distribution function characterizing the noise amplitude, noise sources, frequency dependencies, and convective noise growth.

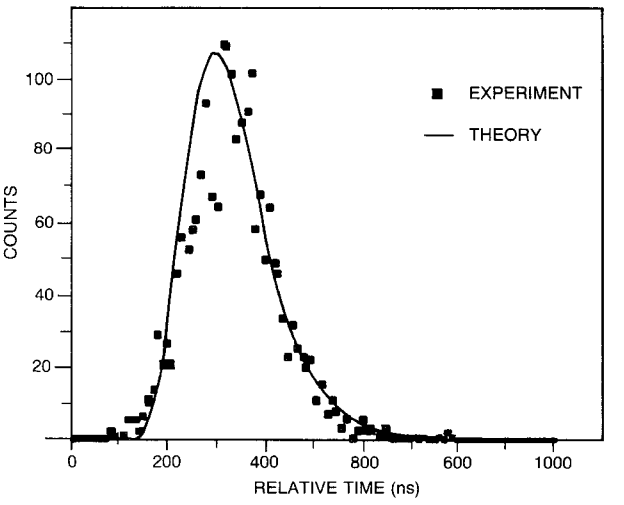


Fig. 7. Distribution function of free oscillation starting times. Solid line indicates Rayleigh distribution with $\tau = 75$ ns.

The exact distribution function of oscillation starting time is measured using an oscillation in the first cavity and no external drive signal. A digitizing oscilloscope displays the gyrotron output as monitored by a crystal diode. A system controller locates a given reference power level on the oscilloscope trace and records the time elapsed from the start of the flat-top portion of the electron beam high voltage pulse. Data gathered from 2000 pulses are displayed on the histogram of Fig. 7. Also drawn on this figure is the distribution $f(t_{\text{ref}})$ from (4). The growth rate is obtained from the oscillation e-folding time on the crystal diode signal. As mentioned previously, the noise power does not affect the shape of the distribution in the undriven case. Hence for this comparison the noise power level need not be known. There is some statistical noise apparent in the data due to the selected bin size (10 ns bins with a 2 ns digitizer resolution), and there is some drifting in the gyrotron oscillation parameters over the time of measurement ( ~ 20 minutes). The agreement between the theory and experiment is nevertheless reasonable. Since the distribution function in (4) comes directly from transformation of the Rayleigh distribution in noise amplitude into the time domain, we can interpret the agreement in Fig. 7 as a confirmation of our assumption that the Rayleigh distribution applies to the free gyrotron oscillator preoscillation noise.

Measurements of the exact starting time distribution function are made as a function of drive power using oscillations in each of the first two cavities. The effect of the external drive on this distribution can be seen in Fig. 8 for an oscillation in the second cavity. The distribution both sharpens and moves toward earlier times as the drive power increases. These trends are also seen in the theory. Similar results were obtained for the first cavity.

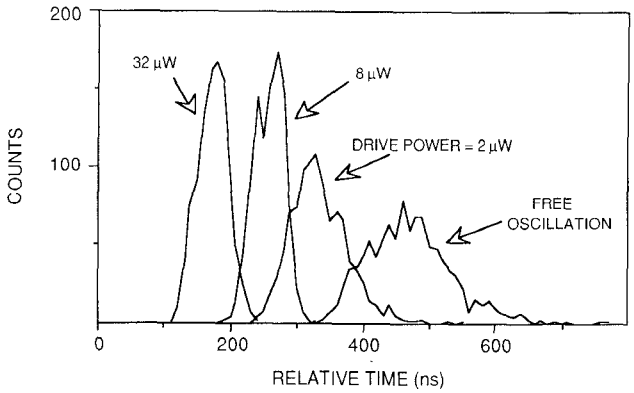


Fig. 8. Change in distribution function of oscillation starting time as a drive signal is applied.

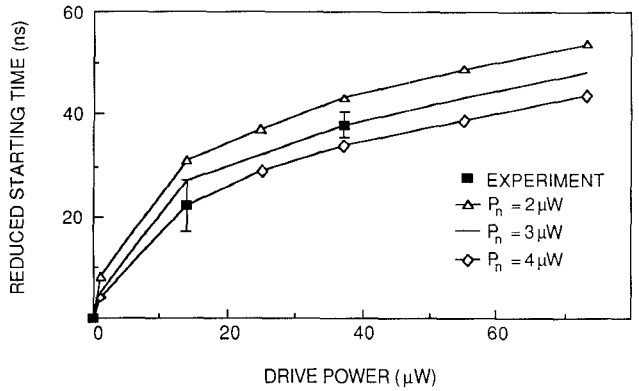


Fig. 9. Decrease in gyrotron oscillation starting time by application of an external signal.

To get a more accurate measure of the preoscillation noise power, the enveloping and averaging techniques outlined previously are used. Though less detailed, these measurements are rapid and hence less susceptible to error through oscillator drift. The only other appreciable error source is the 2 ns resolution limit of the digitizing oscilloscope. A set of these data is shown in Figs. 9 and 10 for an oscillation in the third cavity. The procedure for determining noise power is to simultaneously fit the average starting time and distribution width as a function of drive power. Fig. 9 shows the decrease in oscillation starting time due to the external signal. Also shown are three theoretical curves (from (6)), assuming different noise power levels. The best fit is for a noise power of 3.0 μW. The width of the distribution (between 0.5 percent and 99.5 percent points) is shown in Fig. 10. Again we see the narrowing of the distribution as more drive power is applied. The best fit to the experimental points is again for a noise power of 3.0 μW. The uncertainty in this value is shown by the error bars on the two figures. Preoscillation noise measurements using oscillations in each of the first two cavities (other cavities mechanically tuned far from resonance) result in values near 1.0 μW.

The preoscillation noise power measured here is somewhat larger than expected from common noncollective noise mechanisms. Previous noise measurements in magnetrons have come to the same conclusion (noise power

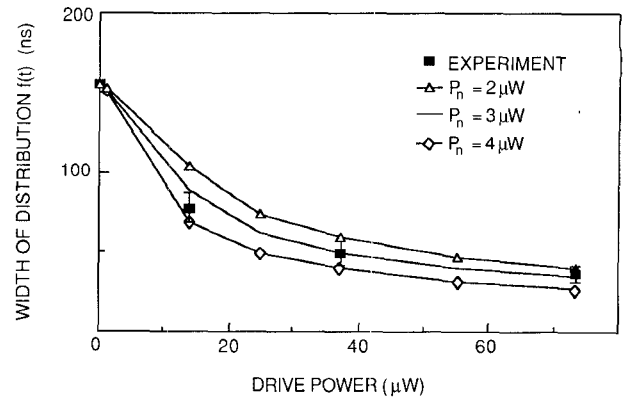


Fig. 10. Reduction in starting time jitter due to application of an external signal.

> 200 mW in [12]). Some common noncollective noise mechansisms are thermal noise, the shot effect, and cyclotron emission.

Noise due to the thermal motion of electrons (Johnson noise) is found in all microwave devices. Using the familiar expression

$$P_n = kTB$$

where $k$ is the Boltzmann constant, $T$ is absolute temperature, and $B$ is bandwidth, one obtains a value of $2.8\times10^{-14}$ W over a bandwidth of 7 MHz. The bandwidth is set by the cavities; thus the thermal noise in the third cavity is about a factor of two larger than stated above. In either case, this thermal noise is over 75 dB below that measured in the experiment.

The noise current at the temperature-limited cathode surface due to the shot effect is [17]

$$i_{\text{rms}}^2 = 2el_0\Delta f$$

where $l_0$ is the dc beam current, $e$ is the electronic charge, and $\Delta f$ is the frequency band over which the measurement is made. The gyrotron cavity filters the possible noise frequencies so that $\Delta f$ is approximately the cavity bandwidth. The noise power is dissipated in the cavity wall and load impedances ($1/G_w$ and the real part of $1/Y_L$, respectively). These quantities are found from measurements of the loaded and unloaded cavity quality factors and the coupling coefficient between the cavity and the load. Assuming a beam–cavity coupling coefficient of 1, and neglecting the effect on the beam of noise fields excited in the external RF circuit, a noise power of $\sim 1.0\times10^{-9}$ W is obtained in the cavity wall resistance. Thus shot noise is about 30 dB below the noise level we experimentally measure.

Cyclotron emission occurs when charges enter a region of magnetic field with a component of velocity perpendicular to the field. The total power radiated by a mildly relativistic rotating electron into the fundamental harmonic can be written [18]

$$P_{\text{cyclotron}} \cong \frac{e^2\omega_b^2}{6\pi\epsilon_0 c}\beta_\perp^2\left[1+\beta_\parallel^2-\frac{7}{5}\beta_\perp^2+\cdots\right]$$

where $\omega_b = eB_0/m$ is the cyclotron angular frequency, $B_0$ is the magnetic field, $m$ is the electron mass, $\beta_\parallel$ and $\beta_\perp$ are the ratios of the axial and perpendicular electron velocities to the speed of light, respectively, and $\epsilon_0$ is the permittivity of free space. Using a beam voltage of 30 kV, a perpendicular-to-parallel beam velocity ratio of 1.5, a beam current of 6 A, and a cyclotron frequency of $4.5 \times 10^9$ Hz, the total power obtained from incoherent cyclotron emission, by linearly adding the power from all electrons in the cavity at a given instant, is 1.2 $\mu$W. This calculation neglects reabsorbtion of radiation by the electrons and coupling losses in the circuit. A crude measurement of cyclotron emission from the first cavity (tuned so as not to oscillate) using a sensitive power meter (100 pW sensitivity) indicated a noise level 10 dB below the calculated value. Thus cyclotron emission seems to be reasonably close to the preoscillation noise observed in the experiment.

Two potential mechanisms of noise growth along the tube are investigated. One is due to the regular gyroklystron amplification mechanism. This mechanism is expected to predominate when the cavities and magnetic fields are tuned so that a beam cyclotron wave can interact with the standing electromagnetic wave in each of the cavities. In addition, it has recently been pointed out that electrostatic beam modes can form and become unstable in gyrating electron beams without interaction with an external RF circuit [19], [20]. These modes, though not yet experimentally observed, should be able to grow both in drift regions and cavities at a rate that can be comparable to that of the electron cyclotron maser instability. This mechanism is then expected to predominate when the cavities are tuned away from the Doppler-shifted relativistic cyclotron frequency of the electron beam.

It is found experimentally that the preoscillation noise power grows along the tube by the gyroklystron mechanism. In the measurements described previously, all cavities but the oscillator were mechanically tuned away from the frequency of interaction. When cavities upstream of the oscillator are tuned to the correct frequency for gyroklystron operation, it is found that the noise power increases. Experiments are done using oscillations in the second cavity (one prebunching cavity) and in the third cavity (two prebunching cavities). The effective small-signal gain is determined in two ways. One is by using the proven numerical gyroklystron code written by Ganguly *et al.* [16]. The other is to experimentally compare the effect on the oscillation of an external signal injected directly into the oscillator with that of a signal into a prebunching cavity. A signal in the prebunching cavity is enhanced by the gyroklystron gain before reaching the oscillator. Because the effects of the small drive signal are felt only during the very early stages of oscillation buildup, it is appropriate to use the full gyroklystron gain up to and including the oscillator cavity. The signal from the prebunching cavity should be more capable of reducing the mean and variance of the oscillator starting time characteristics than the directly injected signal (since the cavities are tuned to provide gyroklystron gain in both cases).

TABLE I

| | drive signal (exp) | drive signal (theo) | noise power |
|---|---|---|---|
| 2-cavity experiment | 20 dB | 19 dB ($\alpha$=1 5) | 15 5 dB |
| 3-cavity experiment | 32 dB | 32 dB ($\alpha$=1 0) | 20 dB |

The gain in the noise power can be determined by inferring noise via direct injection into the cavity oscillator and comparing it with the 1.0 $\mu$W noise power measured in the first cavity. Table I shows these results for typical magnetic field profiles and cavity tuning. As expected, the numerical code predicts the two- and three-cavity signal gain quite well. However the gain of the noise power is not as large. Two possible effects contribute to this smaller gain. One is that the noise power contains all frequencies within the cavity bandwidth. The gyroklystron gain is a function of frequency and drops by about a factor of two near the edges of the cavity band. The other reason is that the preoscillation noise is probably somewhat of an overestimate of the noise present in the beam in the absence of a growing electromagnetic oscillation (for example collective cyclotron emission might occur as the oscillation begins and the electrons begin to bunch in response to the cyclotron radiation field). Evidence for this difference is the noise power measured by Ferguson *et al.* [21] on a gyrotron TWT device using the same MIG gun as in our experiment. Their noise power, measured by shorting the amplifier input and monitoring the output, is about 20 dB below what we measure.

Noise growth due to the electrostatic cyclotron instability (ESCI) is also examined. Our experiment satisfies both of the conditions for instability set forth in [19, eqs. (20) and (22)]. Under the approximations of a cold beam, no dc space charge effects, interaction at the fundamental electron cyclotron frequency, and zero axial wavenumber, the growth rate of the ESCI can be written

$$\omega_i = \beta_\perp \omega_p \frac{|J_1(k_\perp r_L)|}{k_\perp r_L}$$

where $\beta_\perp$ is the beam perpendicular velocity normalized by the speed of light, $\omega_p$ is the plasma frequency, $k_\perp$ is the perpendicular wavenumber, and $r_L$ is the electron Larmor radius. Using the same beam parameters as before, with an annular beam thickness of two Larmor radii, we obtain a gain per unit length of 0.44 dB/cm. The noise should then grow by 6.6 dB from the electron gun to the first cavity, 13.7 dB to the second cavity, and 20.7 dB by the last cavity.

In this experiment all but one of the cavities are tuned away from resonance with the local magnetic field. This effectively decouples the beam from the electrodynamic structure. An important characteristic of the ESCI is that the instability can be totally driven by the beam. By measuring the noise power in the one cavity tuned to resonance, we are able to establish the noise at three locations along the tube. It is found that the noise in the first two cavities is about 1.0 $\mu$W while that in the third is 3.0 $\mu$W. This does not agree with the 6 dB intercavity gain

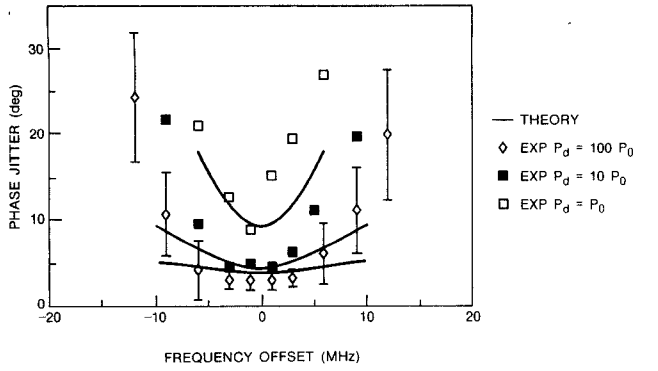


Fig. 11. Phase control of gyrotron by direct injection priming. Experiment compared to theory at three different drive power levels ($P_0$ = 3.83 mW).

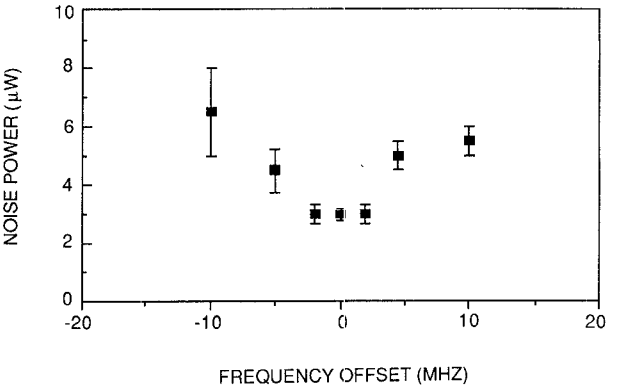


Fig. 12. Dependence of preoscillation noise power measurement on the frequency of the drive signal.

predicted by the theory. Uncertainties in the comparison with theory are that our measurement requires the onset of an oscillation and that some changes in magnetic field profile have to be made to prevent multiple cavity oscillation as the location of the jitter measurement is changed. In addition, the theory only approximately treats the actual experimental conditions of a hollow, cylindrical, confined beam with axial velocity spread. There is uncertainty about the actual coupling strength of the instability to the surrounding circuit as well as about the level at which saturation terminates the instability growth. In the experiment, the instability cannot be simply one dimensional. The effect of nonzero values of axial and azimuthal wave vectors is to increase the RF coupling to the external circuit but may also decrease the growth rate.

### *B. Direct Injection Priming*

Now that the noise power has been determined, the primed gyrotron performance can be predicted. Equations (2) and (14) are used in (12) to evaluate the expected variance in the relative phase angle between the gyrotron and drive signals. Fig. 11 shows the results of direct injection priming of a gyrotron using only the second cavity in the gyroklystron circuit. Due to the tuning of the first cavity and magnetic field, the preoscillation noise power is about 0.1 mW (20 dB above that of the single cavity result). The degree of coherence between the gyrotron and the drive signal is shown on the ordinate as $\arcsin(\sqrt{\chi^2})$. Perfect phase control appears as 0.0 on the ordinate while complete randomness between the two signals is 45°. The general feature exhibited by both the experimental points and the theoretical curves is that of less gyrotron phase control as either the drive power is lowered or the drive frequency is varied from the steady-state gyrotron oscillation frequency. In the theory, the change in phase control with frequency separation occurs because less drive power enters the system, due to the resonance width of the cavity. The theoretical predictions are close to the experimental observations for drive frequencies near that of the gyrotron. The theory, however, overestimates the degree of phase control for frequency separations on the order of the cavity bandwidth. A possible reason for this discrepancy is the failure of the instantaneous priming approximation at large frequency separation.

The instantaneous priming approximation will fail if the external signal is not near the center of the cavity resonance band. This is because for large frquency separations there are large phase slippages between the drive and the oscillator on the time scale for significant growth of the oscillation amplitude. This means that the external signal affects the dynamics of the oscillation buildup rather than merely specifying an initial condition. Using the measured growth time of 43 ns for the second cavity oscillation, the frequency separation at which the instantaneous priming approximation breaks down is about 6 MHz (slippage of $\pi/2$ radians in one growth time). This is similar to the frequency separations at which the theory and experiment begin to seriously disagree in Fig. 11.

One should note that the distribution in starting phase given by (2) is only a function of the mean noise-to-signal power ratio. It is therefore appropriate to generalize our result for direct injection of the second cavity, with an amplified noise level (20 dB above the single cavity result), to direct injection of any cavity in the device regardless of whether or not the noise in that cavity has been amplified. Direct injection of the first cavity, for example, would require 20 dB less drive power than that of our measurement in the second cavity because the noise power level is only 1 μW. However, the signal-to-noise ratio required to reduce phase jitter to a given value would still be the same.

The possibility of drive frequency dependence to our noise measurement was investigated by changing the drive frequency. The results are shown in Fig. 12. The filtering action of the cavity has been taken into account to correct the actual drive signal strength in the cavity. It is seen that our method of determining noise power is not sensitive to drive frequency. The measured changes in noise power across the cavity band are within experimental uncertainties. The apparent sharp rise in noise power at the limits of the cavity bandwidth can be explained once again by the failure of the approximation of instantaneous priming at these frequency separations. In these circumstances the noise power calculation cannot proceed in the manner previously outlined.

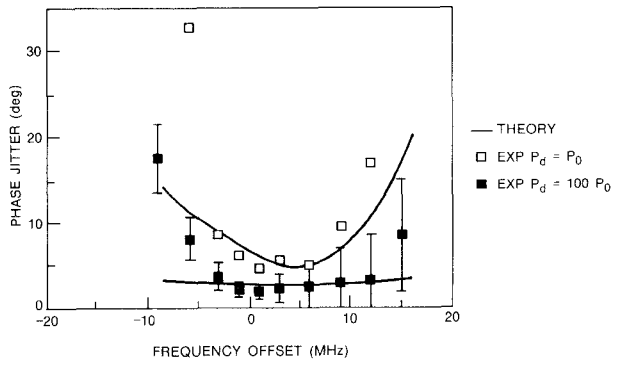


Fig. 13. Phase control of gyrotron by priming via a prebunched beam. Experiment compared to theory at two different drive power levels ($P_0 = 0.0169$ mW).

The advantages of priming as a means of phase control are several. The drive power required to prime an oscillator to a given level of phase control is very low. Phase control to within a phase variance of 2.5° is achieved at a drive-to-oscillator power ratio of −36.6 dB by direct injection (see Fig. 11). This is well below the typical value of −20 dB required for injection phase locking. In addition, the power level required for priming is not directly related to the oscillator power since priming is an effect that takes place during the oscillation buildup. The actual signal-to-noise power ratio required to achieve better than 2.5° phase jitter is 36 dB. Finally the bandwidth over which priming can be an effective means of phase control is large. In Fig. 11, the band over which better than 5° phase control is achieved, for the highest drive power shown, is about twice the cavity bandwidth.

### C. Priming Using a Prebunched Electron Beam

Fig. 13 shows the results of using the external signal to prebunch the electron beam in the first cavity and prime an oscillation in the third cavity. A noise power of 0.10 mW (20 dB above the single-cavity noise power) is used in the theory. The amplification of the drive signal due to the gyroklystron mechanism is given in Table I. The figure shows the same fall off in phase control with decreasing drive power or increasing frequency separation seen in the direct injection experiment. Also, the same discrepancy between experiment and theory is present at large frequency separations, as was noted in the direct injection case. A new feature is that there is better phase control at drive frequencies above that of the free oscillator. This asymmetry is not predicted by the theory. The theory, designed to predict gain and bandwidth of a gyroklystron amplifier, does not predict the frequency of maximum gain to better than about 0.5 percent. In reality, there are frequency shifts, due to beam loading, etc., of this magnitude. It has been found in the experimental gyroklystron amplifier work that the frequency is typically upshifted by 30–45 MHz from the theoretical predictions. This correction has been applied to the results shown in Fig. 13. The general shape of the phase control curves in Fig. 13 do appear quite similar to those seen in the experiment.

The degree of phase control observed in the prebunching experiment is much better than that of any gyrotron or magnetron primed by direct injection. Phase variations of less than 2° are achieved by the three-cavity device at a drive-to-oscillator power ratio of −71 dB. For equivalent control in magnetrons, one requires a power ratio [22] of approximately −20 dB, while the direct injection gyrotron experiment discussed previously required a drive-to-oscillator power ratio somewhat above −36.6 dB. This increase in priming efficiency is due both to the fact that there is more signal gain than noise gain in the gyroklystron circuit and that the noise power level seems to be much smaller in the gyrotron than the magnetron.

Since the noise power does not directly depend on the oscillator power, a more precise comparison between the single- and multicavity systems is made by comparing required drive signal-to-noise power ratios to achieve the same phase control. In the multicavity experiment, the ratio between the drive signal and noise power levels is to be taken at the point where the signal is injected. Thus, in the three-cavity experiment the signal-to-noise is found in the first cavity using a 1 μW noise power. Fig. 13 shows that a phase jitter of less than 2° is maintained at a signal-to-noise power ratio of 22 dB. This is about 15 dB less drive power than required in the direct injection case (36 dB to achieve a jitter of 2.5°). The improvement is predominantly due to the fact that the signal gain is greater than the noise gain. Using the separate gains for the signal and noise power given in Table I, one can find the signal-to-noise ratio in the third cavity from the 22 dB level in the first cavity. The result is a 32 dB effective signal-to-noise level, which is similar to the 36 dB level required by direct injection.

## V. Conclusions

Pulse-to-pulse phase coherence is obtained in the gyrotron by priming. The drive power required for a given degree of phase control is much less (−15 dB) in the prebunched case than by direct injection. A simple theory is constructed which allows the degree of phase control as a function of drive power, noise power, and drive frequency to be predicted. This theory seems to work well for drive frequencies near that of the gyrotron oscillator. The theory also is applied to a three-cavity system and is found to work well if corrections are made for frequency pulling and pushing in the gain section of the device. In addition, the noise power is determined to be ~1.0 μW in the gyrotron. There is no significant noise amplification due to the electrostatic cyclotron instability. All amplification seen can be attributed to the conventional gyroklystron gain mechanism. Greater phase control is achieved using prebunching cavities than by direct injection because the gyroklystron amplification for the noise is less than that of an input signal.

## Acknowledgment

The authors are indebted to W. M. Bollen and J. McAdoo for help in performing the experiment, to A. K. Ganguly for use of the gyroklystron code, and to S.

Swiadek and F. Wood for design and construction of the hardware. Support is also acknowledged from R. K. Parker and V. L. Granatstein.

## REFERENCES


[1] S. Spang *et al.*, "Design and operation of a 200 kW CW, 140 GHz gyrotron oscillator," in *Tech. Dig. IEEE Int. Electron Devices Meeting* (Los Angeles, CA), in 1986, pp. 326–329.

[2] K. E. Kreischer, A. Singh, S. E. Spira, and R. J. Temkin, "Initial operation of a 1 MW, 140 GHz gyrotron," in *Tech. Dig. IEEE Int. Electron Devices Meeting* (Los Angeles, CA), 1986, pp. 330–333.

[3] M. E. Read, K. R. Chu, and A. J. Dudas, "Experimental examination of the enhancement of gyrotron efficiencies by use of profiled magnetic fields," *IEEE Trans. Microwave Theory Tech.*, vol. MTT-30, pp. 42–46, 1982.

[4] E. E. David, Jr., "RF phase control in magnetrons," *Proc. IRE*, vol. 40, pp. 669–685, 1952.

[5] J. C. Slater, "Injection priming of magnetrons," in *Micronotes* (Burlington, MA; Microwave Associates) vol. 4, pp. 2–8, 1966.

[6] A. H. McCurdy *et al.*, "Improved oscillator phase locking by use of a modulated electron beam in a gyrotron," *Phys. Rev. Lett.*, vol. 57, pp. 2379–2382, 1986.

[7] B. Vyse, V. H. Smith, and M. O. White, "The use of magnetrons in coherent transmitters," in *Conf. Proc. Military Microwaves '82* (London, Eng.), 1982, pp. 217–222.

[8] D. M. Guillory and R. W. McMillan, in *Conf. Dig. 10th Int. Conf. Infrared and Millimeter Waves* (Lake Buena Vista, FL), 1985, p. 48.

[9] W. M. Bollen *et al.*, "Design and performance of a three-cavity gyroklystron amplifier," *IEEE Trans. Plasma Sci.*, vol. PS-13, pp. 417–423, 1985.

[10] A. E. Siegman, *Lasers*. Mill Valley, CA: University Science Books, 1986, pp. 1129–1170.

[11] K. A. Norton, L. E. Vogler, W. V. Mansfield, and P. J. Short, "The probability distribution of the amplitude of a constant vector plus a Rayleight-distributed vector," *Proc. IRE*, vol. 43, pp. 1354–1361, 1955.

[12] E. E. David, Jr., "A new method of estimating preoscillation noise in a pulsed oscillator (magnetron)," Tech. Rep. No. 173, MIT Research Laboratory of Electronics, Cambridge, MA, 1950.

[13] B. Vyse and H. Levinson, "The stability of magnetrons under short pulse conditions," *IEEE Trans. Microwave Theory Tech.*, vol. MTT-29, pp. 739–745, 1981.

[14] S. O. Rice, "Mathematical analysis of random noise," *Bell Syst. Tech. J.*, vol. 24, part III, p. 100, 1945.

[15] J. H. Shoaf, D. Halford, and A. S. Risley, "Frequency stability specification and measurement: High frequency and microwave signals," NBS Tech. Note 632, 1973.

[16] A. K. Ganguly, A. W. Fliflet, and A. H. McCurdy, "Theory of multi-cavity gyroklystron amplifier based on a Green's function approach," *IEEE Trans. Plasma Sci.*, vol. PS-13, pp. 409–416, 1985.

[17] S. Goldman, *Frequency Analysis, Modulation and Noise*. New York: McGraw-Hill, 1948, p. 356.

[18] G. Bekefi, *Radiation Processes in Plasmas*. New York: Wiley, 1966, p. 201.

[19] K. R. Chen and K. R. Chu, "Study of a noise amplification mechanism in gyrotrons," *IEEE Trans. Microwave Theory Tech.*, vol. MTT-34, pp. 72–79, 1986.

[20] K. R. Chu and L. Lyu, "Simulation of electrostatic noise amplification in gyrotrons," *IEEE Trans. Microwave Theory Tech.*, vol. MTT-34, pp. 690–695, 1986.

[21] P. E. Ferguson, G. Valier and R. S. Symons, "Gyrotron-TWT operating characteristics," *IEEE Trans. Microwave Theory Tech.*, vol. MTT-29, pp. 794–799, 1981.

[22] J. K. Parker, private communication.


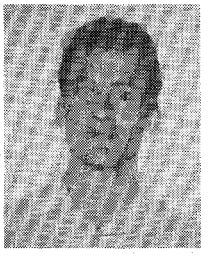

**Alan H. McCurdy** was born in Princeton, NJ, on February 15, 1959. He received the B.S. degree in chemical engineering from Carnegie-Mellon University in 1981 and the B.S. degree in physics from the same institution in 1982. He received the Ph.D. degree in applied physics from Yale University in 1987.

Since 1985 he has worked in the Electronics Science and Technology Division at the Naval Research Laboratory. His research has centered on phase and mode control of gyrotron oscillators.

Dr. McCurdy is a member of the American Physical Society.

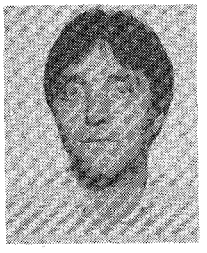

**Carter M. Armstrong** was born in Jersey City, NJ, on November 17, 1950. He received the B.S. degree (with honors) in physics from Rutgers University in 1972 and the Ph.D. degree in physics from the University of Maryland in 1976.

He was on the physics faculty of North Carolina State University from 1977 to 1985. He has been a section head in the Electronics Science and Technology Division at the Naval Research Laboratory since 1985. His research interests include nonneutral plasma interactions and plasma diagnostics.

Dr. Armstrong is a member of the American Physical Society.